

# Holographic SQUID

Shingo Takeuchi

*Shanghai Jiao Tong University, Shanghai 200240, China*

## Abstract

We propose a holographic model of the SQUID (Superconducting QUantum Interference Device) composed of two Josephson junctions connected each other in a circle with the magnetic flux penetrating the circuit of the SQUID and the supercurrents flowing in both Josephson junction. The gravity in this paper is the Einstein-Maxwell-complex scalar field model on the four-dimensional Anti-de Sitter Schwarzschild black brane geometry in which one space direction is compactified into a circle, and we arrange the profile of the coefficient of the time component of the gauge field having the role for the chemical potential of the cooper pair. The magnetic flux is involved by the rewriting of the surface integral of the magnetic field to the contour integral of the gauge field.

# 1 Introduction

In recent years, we have been studying the superconductor using potential applicability of anti-de Sitter (AdS)/conformal field theory (CFT) correspondence [1, 2]. A notable examples are refs.[3, 4, 5], refs.[6, 7, 8] and ref.[9] which have provided the gravity duals for superconductors, (non-)Fermi liquid and a superconductor/insulator transition at zero temperature, respectively.

One of the interesting phenomena associated with the superconductivity would be the Josephson junction [10], and the study of the holographic Josephson junctions is also proceeding. The first paper was ref.[11], in which the superconductor-normal metal-superconductor (SNS) Josephson junction was studied. After that, toward the paper [11], the dimensional extension was discussed in refs.[13, 14] and the generalization to the p-wave Josephson junction was discussed in ref.[15]. Ref.[12] provided the gravity dual for a superconductor-insulator-superconductor (SIS) Josephson junction. In ref.[16], the holographic Josephson junction based on the designer multigravity (namely multi-(super)gravity theories) has been invented

The superconductors in the magnetic fields would also be intriguing, and the holographic study of this has also been proceeding. The first papers would be Refs.[5, 17, 18, 19], and although we cannot refer to all the papers, the papers we have particularly checked in writing of this paper are Refs. [20, 21, 22, 23, 24] besides the above four.

This paper will be devoted to a holographic SQUID (Superconducting QUantum Interference Device) consisted of two Josephson junctions with the magnetic field shown in Fig.1. Here, in Ref.[25], the same type of the holographic SQUID has been considered. In Ref.[25], there is only one supercurrent, despite that originally there are two supercurrents in the SQUID,  $J_L$  and  $J_R$ , as can be seen in Fig.1. However, in Ref.[25], in order to correspond to the two supercurrents in the left and the right sides of the SQUID, how to measure phase differences of the Josephson junctions in the left and the right sides,  $\Delta\theta_L$  and  $\Delta\theta_R$  (For the definitions of these, see Fig.1), is taken skillfully, where the phase differences mean the difference for two phases of the two condensated scalar fields in superconductors. However, their way seems unclear. So, in this paper, another way for the holographic SQUID with the magnetic field is proposed. More detailed introduction to the SQUID and our holographic way to model the SQUID are given in section.2.

Lastly, we mention the organization of this paper. Section.2 is devoted to brief review of the SQUID we will consider in this paper, the points in our holographic way to model the SQUID, which are how to take in the magnetic flux and how to take in the specific behavior of the supercurrent, and the conclusion of this paper. In section.3, we give our gravity model and the equations of motion. Further, we mention about the ansatz. In section.4, we show the results of our analysis in the holographic SQUID of ours. In Appendix A,

we list the numerical results used in section.4 explicitly.

## 2 Brief review of SQUID, our holographic way to model it and conclusion

We devote this section to brief review of the SQUID we consider in this paper and the points in our holographic way to model it.

### 2.1 Brief review of SQUID in this paper

The SQUID we consider in this paper is given by connecting two Josephson junctions in a circle and attaching two branches as the gateway for the inflowing and outflowing supercurrents as shown in Fig.1.

Then, the supercurrents flowing in the left and the right Josephson junctions in the loop of SQUID are generally known to be given as  $J_L \equiv I_{cL} \sin \Delta\tilde{\theta}_L$  and  $J_R \equiv I_{cR} \sin \Delta\tilde{\theta}_R$  respectively (we obtain such a sine relation later as in Fig.7), where we have defined the gauge invariant phase differences as  $\Delta\tilde{\theta}_L \equiv -\frac{e^*}{\hbar} \int_a^b \mathbf{A} \cdot d\mathbf{l} + \Delta\theta_L$  and  $\Delta\tilde{\theta}_R \equiv -\frac{e^*}{\hbar} \int_c^d \mathbf{A} \cdot d\mathbf{l} + \Delta\theta_R$ , where  $d\mathbf{l}$  means the line elements. As a result, the total amount of these two is equal to the inflowing supercurrent  $J_{\text{total}}$  as

$$\begin{aligned} J_{\text{total}} &= J_L - J_R \\ &= 2J_c \cos\left(\frac{\Delta\tilde{\theta}_L + \Delta\tilde{\theta}_R}{2}\right) \sin\left(\frac{\Delta\tilde{\theta}_L - \Delta\tilde{\theta}_R}{2}\right), \end{aligned} \quad (2.1)$$

where we have assumed  $J_{cL} = J_{cR} \equiv J_c$  for simplicity (this assumption is usually taken in the texts of condensed matter physics) and changed the sign of  $J_R$  taking into account of the fact that we measure the phases

in anticlockwise direction in the circuit of Fig.1. Then, the contour integral of the phase  $\nabla\theta$  along the circuit of the SQUID is given by integral multiplication of  $2\pi$  as  $2\pi n = \oint \nabla\theta \cdot d\mathbf{l}$ , which leads the relation:

$$2\pi n = 2\pi \frac{\Phi}{\Phi_0} + \Delta\tilde{\theta}_L + \Delta\tilde{\theta}_R, \quad (2.2)$$

where  $n$  is integer numbers and it turns out that  $\nabla\theta$  is given as  $\nabla\theta = (m^*\mathbf{v}_s + e^*\mathbf{A})/\hbar$  ( $\mathbf{v}_s$ ,  $m^*$  and  $e^*$  are the velocity, the mass and the electric charge of a cooper pair forming the supercurrents). Further, and  $\Phi_0$  means some constant  $\Phi_0 \equiv h/e^*$  and  $\Phi$  means the magnetic flux penetrating the circuit of the SQUID as  $\Phi = \int (\nabla \times \mathbf{A}) \cdot d\mathbf{S}$ , where  $d\mathbf{S}$  means the area elements. Here, to derive the above relation,  $\mathbf{v}_s = 0$  is

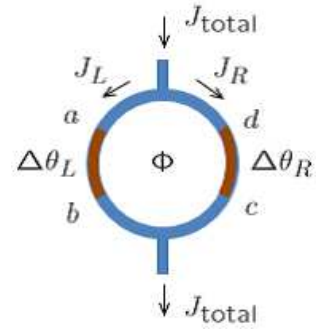


Figure 1: The figure of the SQUID we consider in this paper. The blue and the brown parts represent the superconductor and the normal metal parts, respectively.  $\Delta\theta_L$  and  $\Delta\theta_R$  represent the phase difference in the intervals of the normal metal parts  $a-b$  and  $c-d$ .  $J_L$  and  $J_R$  represent the supercurrents flowing in the left and the right sides.  $\Phi$  represents the magnetic flux penetrating the circuit.

taken in the superconductor part of the circuit of the SQUID by assuming that the path of the integration goes through the center of the section of the circuit. The validity of this  $\mathbf{v}_s = 0$  can be known from London equation and Maxwell equation. Then, using the relation (2.2), eq.(2.1) can be rewritten as

$$J_{\text{total}} = J_{\text{max}}(\Phi) \sin \left( \Delta\tilde{\theta}_L + \pi \frac{\Phi}{\Phi_0} \right) \quad \text{with} \quad J_{\text{max}}(\Phi) \equiv 2J_c \cos \left( \pi \frac{\Phi}{\Phi_0} \right), \quad (2.3)$$

where the above has been obtained with  $n = 0$  in eq.(2.2). The behavior of  $J_{\text{max}}(\Phi)$  against the magnetic flux  $\Phi$  is one of the specific behavior of SQUID, and we will aim to reproduce it in our holographic SQUID (Fig.8).

## 2.2 Our holographic SQUID

Now that we have reviewed the condensed matter physics side, we will turn to the points in our holographic way to model the SQUID, which are how to take in the magnetic flux and how to consider the flow of the supercurrent. Explicit descriptions of our model is presented after this section.

The background geometry in this paper will be the four-dimensional Anti-de Sitter Schwarzschild black brane geometry. Then, the boundary space is given as 1+2 dimensional space. We compactify a direction of the two space directions into a  $S^1$  circle, which means that the boundary space in this paper is given as the surface of the cylinder. We illustrate the boundary space in Fig.2 on which some our dual field theory lives.



Figure 2: This figure illustrates the boundary space on which the dual field theory is. Here, our boundary space is given not as the cylinder including its interior, but as the surface of the cylinder. We refer to the circled direction as  $\chi$ -direction. Then, we put our holographic SQUID on  $\chi$ -direction in the form of the loop.  $\Phi$  represents the magnetic flux running in the interior of the cylinder, which itself is fictitious (due to the absence of the interior space) but finally we can take in the effect of the magnetic flux  $\Phi$  by the rewriting of the surface integral of the magnetic field to the contour integral of the gauge field [23, 24] as mentioned in the body text.

We realize our holographic SQUID on the  $S^1$  circled space in the form that it winds around the  $S^1$  circle. The SQUID is composed of two Josephson junctions as can be seen in Fig.1. Then, to model such double holographic Josephson junctions, we arrange the time component of the gauge field appropriately by exploiting its  $\chi$  dependence as in eq.(3.12) as well as Ref.[11], where the coefficients appearing in the expansion around the horizon are known to have the roles of the density (charge) and the chemical potential

conjugate to that density (charge), (ref.[27] would be one of good papers for this matter). In what follows, we refer the circled direction as  $\chi$ -direction. For more concrete description, see Section.3.

Here, we mention one of the issues in our holographic model, which is how to take in the magnetic flux. First, the space of the dual field theory does not include the interior space of the cylinder. Hence, the magnetic flux penetrating the loop of the SQUID cannot exist in the dual field theory. However, temporarily considering the interior space of the cylinder in the space of the dual field theory, let us assume that the magnetic flux  $\Phi$  given as  $\Phi = \int d\mathbf{S} \cdot \mathbf{B}$  exists. Then, considering the external gauge field  $a_\chi(\chi)$  in the space of the dual field theory on the surface of the cylinder,  $\Phi$  can be rewritten using the Stokes's theorem as  $\Phi = \oint_\chi d\chi a_\chi(\chi)$ . Here, denoting  $\nu(\chi)$  as the coefficient of the  $\chi$  component of the gauge field in the vicinity of the boundary in the bulk gravity, it is known that  $\nu(\chi)$  and  $a_\chi(\chi)$  can correspond each other through GKP-W relation (Gubser, Klebanov, Polyakov and Witten) [2]. Then, we can link the magnetic flux  $\Phi$  we have spuriously assumed to the external gauge field  $\nu(\chi)$  actually existing as

$$\Phi = \oint_\chi d\chi \nu(\chi). \quad (2.4)$$

Hence, in the conclusion, despite that we cannot have the magnetic flux itself, we can fictitiously take in the effect of the magnetic flux. Finally, this way using the rewriting of the surface integral of the magnetic field to the contour integral of the gauge field has been performed in refs.[23, 24].

We have another issue, which is the effect coming from the branches appeared in Fig.1. If there is the branches, the current inflows from the above, separates into two flows, and finally outflows to the below. On the other hand, if it were not for the branches, the circuit of the SQUID would become a simple loop and the supercurrent simply circulate in the circuit of the SQUID. Hence, since there is no branch in our holographic model of the SQUID, our holographic SQUID is just a loop consisted of two Josephson junctions.

If we try to take in the effect of the branches, we have to consider the boundary condition such that all the fields in three sectors, the left, the right and the branch parts, connect continuously each other at the joint parts between the circuit and the branches. However, the calculation involving such a boundary condition is difficult more than we can handle. Hence, in this paper, considering that there is no continuous condition at the joint parts in the circuit of the SQUID in Fig.1, the SQUID we consider is the one without the branches and separated into the left and the right parts as in the left figure of Fig.3, where the meaning of the separation is mentioned in the following.

Here, we mention the reason for no continuous condition. Since the supercurrent suddenly splits or joins at the joint parts, the amount of supercurrent varies rapidly, which would be mostly discontinuous. Therefore, we can simply consider that the fields at the joint parts are discontinuous.

Next, we mention about separating into the left and the right parts in Fig.3. Since there is no continuous condition as mentioned above, we can consider that there is no interference between the two Josephson junctions. Therefore, we perform the analysis not for the two Josephson junctions interfering each other but for a Josephson junction solitarily.

Then, we mention how to obtain the result of the SQUID from such two independent Josephson junctions. First, we assume that we have obtained the results for one Josephson junction with no interfering with the other Josephson junction. Actually, it is presented in Fig.7, where the numerical data for it is presented in Table.1 of Appendix A. Then, we choose the value of the supercurrents from Table.1 and simply treat these as the amount of supercurrent flowing in the each side. Accompanying this, the phase differences in each Josephson junctions are chosen, which gives the magnetic flux penetrating the circuit of the SQUID. Then, now that we have the information of the supercurrents in each sides and the magnetic flux, we can obtain the values of  $J_{\max}(\Phi)$  in eq.(2.3), and finally obtain the results of the SQUID, which is Fig.3.

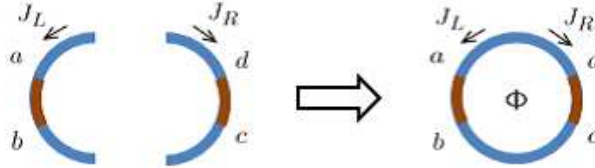


Figure 3: This figure illustrates conceptually that we simply consider the circuit of the SQUID as the one except for the branches, and separate it into the left and the right parts. Then, performing the analysis in each side one by one separately, finally we consider the result of a SQUID by simply joining the results of these two analyses.

Although this analysis is a calculation of two Josephson junctions which has already been done in ref.[11], by this analysis, we can catch the characteristic point of the SQUID.

### 3 Holographic setup to model SQUID

We will consider in this paper the following action as

$$S = \int d^4x \sqrt{-g} \left[ R + \frac{6}{L^2} - \frac{1}{4} F_{\mu\nu} F^{\mu\nu} - |D\psi|^2 - m^2 |\psi|^2 \right], \quad (3.1)$$

where  $\mu, \nu = 1, \dots, 4$ ,  $A_\mu$  is the U(1) gauge field and  $F_{\mu\nu} = \partial_\mu A_\nu - \partial_\nu A_\mu$ . Further,  $D_\mu \equiv \nabla - iqA_\mu$  and  $m^2 = -2$ . We will take the probe approximation in our analysis, which can be obtained by rescaling  $\psi = \tilde{\psi}/q$ ,  $A = \tilde{A}/q$  and taking  $q \rightarrow \infty$  with keeping  $\tilde{\psi}$  and  $\tilde{A}$  fixed.

One of the solutions in the model (3.1) is the four-dimensional Anti-de Sitter Schwarzschild black brane geometry,

$$ds^2 = -f(r)dt^2 + \frac{1}{f(r)}dr^2 + r^2(dx^2 + d\chi^2), \quad (3.2)$$

where  $f(r) \equiv r^2 (1 - r_0^3/r^3)$  with the location of the horizon  $r_0$ .  $\chi$ -direction is  $S^1$  compactified with the periodicity  $-\pi R \leq \chi \leq \pi R$  with  $\pi R = 7$  (For convenience in our actual analysis, we have come to take such a odd number). Here, Hawking temperature is given as  $T = \frac{3r_0}{4\pi L^2}$ . We have fix the AdS radius  $L$  as  $L = 1$ . Further, as written under eq.(3.8), we will fix  $r_0$  as  $r_0 = 1$ . As a result, the temperature to be considered in this paper finally is  $T = 3/(4\pi)$ .

Here, let us give a comment on another geometry. The soliton geometry [26] is also one of solutions in the model (3.1). However, in the case of the soliton geometry, due to the vacuum current and the difference in the fluxoid number [23], the things are much involved. Therefore, in this paper, we will fix the background geometry to the black brane geometry shown above, and the boundary space is given as a surface of a cylinder. Here, it is known in ref.[9] that the black brane geometry (3.2) is energetically favorable toward the soliton geometry provided that  $T > 1/(2\pi R)$ , where  $R$  in this paper is taken as  $R = 7/\pi$ .

All the fields are, as an ansatz, functions of  $r$  and  $\chi$  and the forms of these are given as

$$\tilde{\psi}(r, \chi) = \bar{\psi}(r, \chi) e^{i\varphi(r, \chi)}, \quad (3.3)$$

$$\tilde{A}(r, \chi) = A_t(r, \chi) dt + A_r(r, \chi) dr + A_\chi(r, \chi) d\chi, \quad (3.4)$$

where  $|\psi|$ ,  $\varphi$ ,  $A_t$ ,  $A_r$ , and  $A_\chi$  are realistic function of  $r$  and  $\chi$  and periodic for  $\chi$ -direction as  $\tilde{\psi}(r, \chi + 14) = \tilde{\psi}(r, \chi)$  and  $\tilde{A}(r, \chi + 14) = \tilde{A}(r, \chi)$ , but, not continuous at  $\chi = 0, \pm 7$  for the reason mentioned in subsection.2.2, where the branches as in Fig.1 attach at  $\chi = 0, \pm 7$ . In the following, we will work with the gauge-invariant quantity  $M_\mu \equiv A_\mu - \partial_\mu \varphi$  as well as Ref. [11].

### 3.1 Equations of motion

We can obtain the equations of motion as

$$\frac{\partial_\chi^2 M_t(r, \chi)}{r^2 f(r)} - \frac{2M_t(r, \chi)\rho(r, \chi)^2}{f(r)} + \frac{2\partial_r M_t(r, \chi)}{r} + \partial_r^2 M_t(r, \chi) = 0, \quad (3.5a)$$

$$-\partial_\chi^2 M_r(r, \chi) + 2r^2 M_r(r, \chi)\rho(r, \chi)^2 + \partial_r \partial_\chi M_\chi(r, \chi) = 0, \quad (3.5b)$$

$$-\frac{f'(r)\partial_\chi M_r(r, \chi)}{f(r)} + \frac{f'(r)\partial_r M_\chi(r, \chi) - 2M_\chi(r, \chi)\rho(r, \chi)^2}{f(r)} - \partial_r \partial_\chi M_r(r, \chi) + \partial_r^2 M_\chi(r, \chi) = 0, \quad (3.5c)$$

$$\begin{aligned} & \left( \frac{f'(r)}{f(r)} + \frac{2}{r} \right) \partial_r \rho(r, \chi) - \frac{m^2 \rho(r, \chi)}{f(r)} + \frac{M_t(r, \chi)^2 \rho(r, \chi)}{f(r)^2} - \frac{M_\chi(r, \chi)^2 \rho(r, \chi)}{r^2 f(r)} \\ & + \frac{\partial_\chi^2 \rho(r, \chi)}{r^2 f(r)} - M_r(r, \chi)^2 \rho(r, \chi) + \partial_r^2 \rho(r, \chi) = 0, \end{aligned} \quad (3.5d)$$

$$\begin{aligned} & f'(r)M_r(r, \chi)\rho(r, \chi) + f(r)\partial_r M_r(r, \chi)\rho(r, \chi) + 2f(r)M_r(r, \chi)\partial_r \rho(r, \chi) \\ & + \frac{2f(r)M_r(r, \chi)\rho(r, \chi)}{r} + \frac{\partial_\chi M_\chi(r, \chi)\rho(r, \chi)}{r^2} + \frac{2M_\chi(r, \chi)\partial_\chi \rho(r, \chi)}{r^2} = 0. \end{aligned} \quad (3.5e)$$

where  $'$  means the derivative with regard to  $r$ . Here, it tunes out that there is a relation among above equations of motion as  $\partial_r (f \cdot \text{eq.}(3.5b)) - \partial_\chi (f \cdot \text{eq.}(3.5c)) = 2r^2 \bar{\psi} \cdot \text{eq.}(3.5e)$ . Hence, we can see that both the

number of independent equation in the above and the number of variable appearing in the above equations are four. Here, the above are equations of motion with regard to the fields associated with  $|\psi|$ , and the equation of motion with regard to  $A_x$  has decoupled. Now, for the simplicity in the expansion of the fields around the boundary, we rescale the fields as

$$\rho(r, \chi) \rightarrow \frac{\rho(r, \chi)}{r^{(3-\sqrt{9+4m^2})/2}} \quad \text{and} \quad M_r(r, \chi) \rightarrow \frac{M_r(r, \chi)}{r^2}. \quad (3.6)$$

Then, the above equations of motion can be rewritten as

$$\frac{2 \left(\frac{1}{z}\right)^{\sqrt{4m^2+9}-1} M_t(z, \chi) \rho(z, \chi)^2}{z^3 - 1} + \frac{\partial_\chi^2 M_t(z, \chi)}{1 - z^3} + \partial_z^2 M_t(z, \chi) = 0, \quad (3.7a)$$

$$-2 \left(\frac{1}{z}\right)^{\sqrt{4m^2+9}-1} M_r(z, \chi) \rho(z, \chi)^2 + \partial_\chi^2 M_r(z, \chi) + \partial_z \partial_\chi M_\chi(z, \chi) = 0, \quad (3.7b)$$

$$\begin{aligned} \frac{2 \left(\frac{1}{z}\right)^{\sqrt{4m^2+9}-1} M_\chi(z, \chi) \rho(z, \chi)^2}{z^3 - 1} + \frac{3z^2 \partial_\chi M_r(z, \chi)}{z^3 - 1} + \partial_z \partial_\chi M_r(z, \chi) \\ + \frac{3z^2 \partial_z M_\chi(z, \chi)}{z^3 - 1} + \partial_z^2 M_\chi(z, \chi) = 0, \end{aligned} \quad (3.7c)$$

$$\begin{aligned} \frac{(-(\sqrt{4m^2+9}-4)z^3 + \sqrt{4m^2+9}-1) \partial_z \rho(z, \chi)}{z(z^3-1)} - \frac{(-2m^2 + 3\sqrt{4m^2+9}-9)z \rho(z, \chi)}{2(z^3-1)} \\ + M_r(z, \chi)^2(-\rho(z, \chi)) + \frac{M_t(z, \chi)^2 \rho(z, \chi)}{(z^3-1)^2} + \frac{M_\chi(z, \chi)^2 \rho(z, \chi)}{z^3-1} + \frac{\partial_\chi^2 \rho(z, \chi)}{1-z^3} + \partial_z^2 \rho(z, \chi) = 0, \end{aligned} \quad (3.7d)$$

$$\begin{aligned} -\frac{1}{2} \left\{ \left( \sqrt{4m^2+9}-4 \right) z^3 - \sqrt{4m^2+9} + 1 \right\} M_r(z, \chi) \rho(z, \chi) + \frac{1}{2} z (z^3-1) \partial_z M_r(z, \chi) \rho(z, \chi) \\ + z (z^3-1) M_r(z, \chi) \partial_z \rho(z, \chi) + \frac{1}{2} z \partial_\chi M_\chi(z, \chi) \rho(z, \chi) + z M_\chi(z, \chi) \partial_\chi \rho(z, \chi) = 0. \end{aligned} \quad (3.7e)$$

Here, we have changed the radial coordinate as  $z \equiv 1/r$ .

### 3.2 Solutions around the horizon and the boundary

We can see that the equations of motion (3.5a)-(3.5e) are invariant under the following rescaling,

$$(t, \chi, \rho, r) \rightarrow (t/a, x/a, \rho/a, ar), \quad (3.8)$$

$$(M_t, M_\chi, M_\rho, M_r) \rightarrow (M_t/a, M_x/a, M_\rho/a, a M_r), \quad (3.9)$$

where  $a$  is a rescaling parameter we use here temporary. In our actual analysis, we fix this scale invariance such that  $z_0 (\equiv 1/r_0) = 1$ .

Then, the expansions of the solutions near the boundary are turned out to be given as

$$\bar{\psi}(z, \chi) = \bar{\psi}^{(1)}(\chi) + \bar{\psi}^{(2)}(\chi) z^{\sqrt{9+4m^2}} + \mathcal{O}(z^{2\sqrt{9+4m^2}}), \quad (3.10a)$$

$$M_t(z, \chi) = \mu(\chi) - \rho(\chi)z + \mathcal{O}(z^2), \quad (3.10b)$$

$$M_r(z, \chi) = M_r^{(1)}(\chi)z + \mathcal{O}(z^2), \quad (3.10c)$$

$$M_\chi(z, \chi) = \nu(\chi) + J(\chi)z + \mathcal{O}(z^2). \quad (3.10d)$$



Here, in the dual field theory,  $\mu(x)$  and  $\rho(x)$  have the role as the chemical potential and the density for the Cooper pair. On the other hand,  $\nu(x)$  and  $J(x)$  have the role of the one associated with the magnetic flux as in eq.(2.4) and the supercurrent of the Cooper pair. We take up  $\mu(x)$  in more detail shortly again. Next, with regard to  $\bar{\psi}^{(1)}(\chi)$  and  $\bar{\psi}^{(2)}(\chi)$ , the existence of  $\bar{\psi}^{(1)}(\chi)$  leads the term  $\bar{\psi}^{(1)}(\chi)\bar{\psi}^{(2)}(\chi)$  in the field theory side of the GKP-W relation [2], and the existence of that term breaks the  $U(1)$  global symmetry in the dual field theory is broken. For this reason, we have taken  $\bar{\psi}^{(1)}(\chi)$  to zero. Then,  $\bar{\psi}^{(2)}(\chi)$  will have the role of the wave function of the Cooper pair in the boundary theory.

Then, let us turn to  $\mu(\chi)$  in more detail. It is generally known in the GKP-W relation [2] that  $\mu(\chi)$  has a role of the chemical potential for the Cooper pair, and we set  $\mu(\chi)$  as

$$\mu(\chi) = \mu_L(\chi) + \mu_R(\chi) \quad (3.11)$$

with

$$\mu_L(\chi) = \mu_H - \lambda \left[ \tanh \left\{ \frac{\kappa(\chi - \delta + \epsilon)}{\pi} \right\} - \tanh \left\{ \frac{\kappa(\chi - \delta - \epsilon)}{\pi} \right\} \right], \quad (3.12)$$

$$\mu_R(\chi) = \mu_H - \lambda \left[ \tanh \left\{ \frac{\kappa(\chi + \delta + \epsilon)}{\pi} \right\} - \tanh \left\{ \frac{\kappa(\chi - \delta - \epsilon)}{\pi} \right\} \right]. \quad (3.13)$$

Here  $\kappa$  has the role of roundness,  $\delta$  has the role of position,  $\epsilon$  has the role of width and  $\lambda$  has the role of depth and  $\mu_H$  has the role of height. Here,  $\lambda$  is in the following relation:  $\mu_H - 2\lambda = \mu_L$ , where  $\mu_L$  appears later.

In the actual calculations in this paper, we always set  $\mu(\chi)$  as in shown in Fig.4, where we assume in the figure that the branch parts as in Fig.1 locate at  $\chi = 0$  and  $\pm 7$ . Here, let us notice that, in Fig.4 taking into account of the fact that we measure the phases in anticlockwise direction in Fig.1, the right and the left figures correspond to the chemical potentials in the left and the right parts in the SQUID. By setting so, we perform our analysis for each side one by one separately with giving the various values of supercurrents flowing in the left and the right sides as the initial values. It means that, there being the stage where the supercurrent flowing into the left and the right sides are determined from the configuration of the Josephson junctions in the left and the right sides and the amount of the supercurrent flowing into the SQUID, such a stage is skipped in our analysis. We mention the validity for this skip in section 2.2.

Then, simply joining the results of each Josephson junction, we read out the results as the results of a SQUID. In what follows, let us mention the condition that the profile of the chemical potential should satisfy to model a Josephson junction.

We have set the temperature to  $T = 3/(4\pi)$  using the rescaling as in eq.(3.8). Then, since the ratios  $T/\mu$  and  $T/T_c$  are invariant under this scale transformation (The critical temperature  $T_c$  means the one for

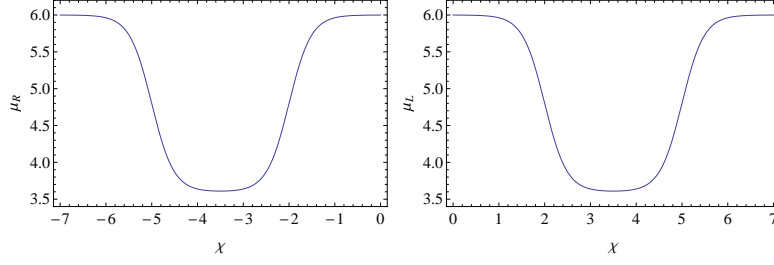


Figure 4: An example of the profile of the chemical potential given in eq.(3.12) with the parameters:  $\mu_H = 6.0$ ,  $\kappa = 6.5$ ,  $\delta = 3.5$ ,  $\epsilon = 1.5$  and  $\lambda = 1.2$ . Here,  $\chi$ -direction is  $S^1$  compactified with the period 14 and  $m^2 = -2$ . Although we show two figures here, these are indeed connected in  $S^1$  circled space, where we assume the branch parts as in Fig.1 locate at  $\chi = 0$  and  $\pm 7$ , from which the supercurrents flow in and flow out. Why we show a profile as two profiles separately is that we perform the analysis for each one independently for the reason mentioned in section 2.2. Here, notice that, taking into account of the fact that we measure the phases in anticlockwise direction in Fig.1, the right and the left figures correspond to the chemical potentials in the left and the right parts in the SQUID.

the superconductor/normal metal transition), the effect of temperature is given from these ratios. However, since the chemical potential in our paper is not constant, it is impossible that the roles of temperature and the chemical potential exchange each other. As a result, we cannot take in the effect of temperature from the ratio of  $T/\mu$ . Hence, we will take the ratio  $T/T_c$  to take in the effect of temperature. Then, let us show the critical temperatures in our paper.

As can be seen in Fig.4, in the profile of our chemical potential, there are higher and lower sections. @ Then, writing the values of these sections as  $\mu_H$  and  $\mu_L$ , the critical temperature for each chemical potential are known to be given as  $T_{cH} = c \mu_H$  and  $T_{cL} = c \mu_L$  with  $c \equiv 0.0588$  [11]. Here, when temperature is higher than the critical temperature, the phase in that section is in normal phase and vice versa. Hence, in order to model a Josephson junction holographically, we should take the temperatures  $T_{cL}$  and  $T_{cH}$  such that  $T_{cL} < T < T_{cH}$ , which can be written as  $\frac{\mu_L}{\mu_H} < \frac{T}{c \mu_H} < 1$ , where  $T$  is now fixed as  $T = 3/(4\pi)$  as mentioned above.

## 4 The analyses and the results

Taking the chemical potential  $\mu$  for each side separately as in Fig.4, we numerically solve the equations of motion (3.7a)-(3.7e) twice with various  $J$  as the inputs of the numerical calculation. Namely, our analysis is the one which performs two calculations for a Josephson junction. In our solving, we impose the boundary conditions  $M_t|_{z=z_0} = 0$  and that  $M_r$  is odd function and  $M_t$ ,  $M_\chi$  and  $|\Psi|$  are even functions for  $\chi$ -direction, where  $\chi$ -direction is the half space of the whole  $\chi$  space, since we perform the calculation for each side of the chemical potential in each side of the circuit of the SQUID separately. To this purpose, we use the spectral method on the Chebyshev Grid [28]. We show examples of the solutions we have obtained in Fig.5.

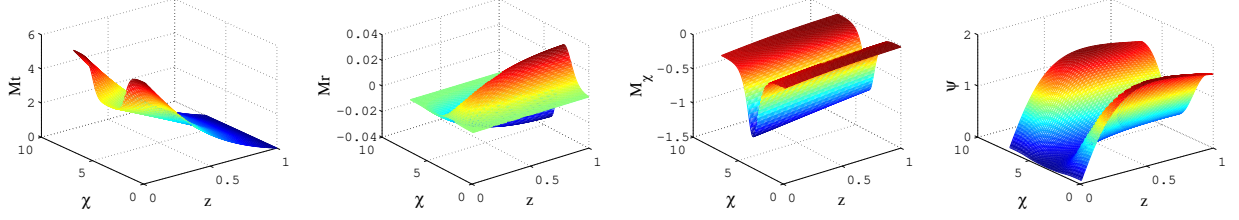


Figure 5: These figures represent examples for the solutions of  $M_t$ ,  $M_r$ ,  $M_\chi$  and  $|\psi|$  obtained in the parameters as follows.  $J/T_{\text{cH}}^2 = 1.21316$ . The chemical potential (3.12) taken in this calculation is same with the one in the right figure of Fig.4. The Chebyshev Grid is taken as  $(n_z, n_\chi) = (23, 45)$ , where  $n_z$  and  $n_\chi$  mean number of the grid in  $z$ - and  $\chi$ -directions. Here, these calculations are performed in the half of the whole *chi* space since our calculations are performed for the left and the right parts in the circuit of the SQUID one by one separately. We show how the sections of the solutions of  $|\psi|$  and  $M_\chi$  at the boundary,  $z = 0$ , in Fig.6, which mean the condensation of the cooper pair and  $\chi$  component of the gauge field in the dual field theory, respectively.

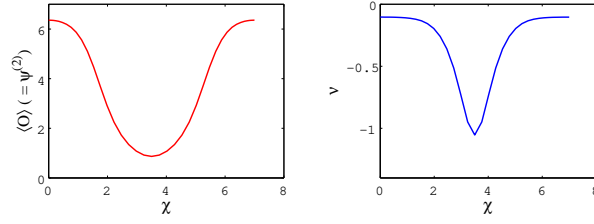


Figure 6: These two figures represent the sections of the solutions of  $\overline{\psi}^{(2)}$  and  $M_\chi$  at the boundary,  $z = 0$ , which mean the condensation of the cooper pair  $\langle \mathcal{O} \rangle$  and  $\chi$  component of the gauge field in the dual field theory, respectively.

Finally, we can obtain the numerical results shown in Fig.7, where we list the numerical results of the calculations explicitly in Table.1. The dashed line in the figure is the guide for the eye to show that our results are on a sine curve, which is  $J_L/(T_{\text{cH}})^2 = 1.1935 \sin(\gamma_L)$ . The result on the sine curve like Fig.7 is one of the specific behavior in a Josephson junction.

In Fig.7, we can see that the section of  $x$ -axis is in from about  $-\pi/2$  to  $\pi/2$ . The reason for that is that we could not find any solutions outside of that region in our numerical calculation. This situation is same with Refs.[11, 12].

Here, we mention how to measure the phase difference in this paper. Here, the description and idea in this paragraph has been proposed first in ref.[11]. The phase difference is usually defined in the gauge invariant way as  $\gamma \sim \Delta\varphi - \int A$ , where the integral region is over an normal phase part. However, since the edges of our junctions are not sharp to avoid problems in numerical analysis, this phase difference is not convenient. Instead, in this study, we will define the following phase difference for the left and the right sides respectively as

$$\gamma_L \equiv \int_0^7 d\chi (\nu(\chi) - \nu(0)) \quad \text{and} \quad \gamma_R \equiv \int_{-7}^0 d\chi (\nu(\chi) - \nu(-7)). \quad (4.1)$$

Here, we have taken into account of the fact that we measure the phases in anticlockwise direction in the

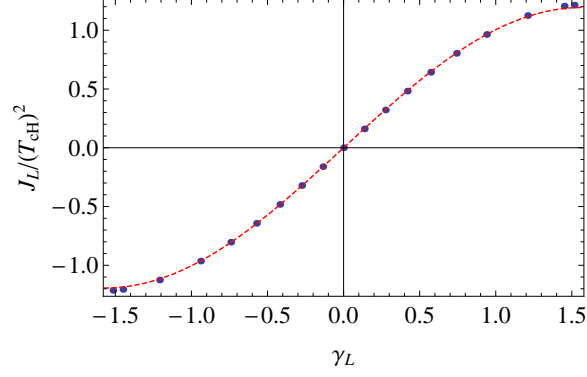


Figure 7: The blue points mean our numerical result obtained from solving the equations of motion (3.7a)-(3.7e) with the chemical potential  $\mu$  given in the right figure in Fig.4 and various  $J_L$  as the inputs of the numerical calculations. Here,  $x$ - and  $y$ -axes mean the phase difference  $\gamma_L$  given in eq.(4.1) and the supercurrent  $J_L$  normalized by  $T_{cH}^2$ , where  $T_{cH} \equiv c \mu_H$  with  $c \equiv 0.0588$  [11]. The dashed line is the guide for the eye to show that these results are on a sine curve, which is  $J_L / (T_{cH})^2 = 1.1935 \sin(\gamma_L)$ . The result on a sine curve like this figure is one of the specific behavior in a Josephson junction. We can see that the section of  $x$ -axis is in from about  $-\pi/2$  to  $\pi/2$ . The reason for that is that we could not find any solutions outside of that region in our numerical calculation, which is same situation with Refs.[11, 12].

circuit of the SQUID in Fig.1.

Having obtained the result in a Josephson junction, let us turn to the holographic SQUID. The holographic SQUID we consider is a combination of Josephson junctions made of the chemical potential given in Fig.4. To begin with, let us use  $J_L$  and  $J_R$  to denote the supercurrents flowing in the left and the right sides in the circuit of the SQUID as in Fig.1, respectively. Then, considering the circuit of the SQUID separately as in Fig.3, we set various values of  $J_L$  as in Table.1 with a fixed  $J_R = -0.482052$ . Here, this  $J_R$  means the current flowing from the top to the bottom in Fig.1, since we define the  $J_{\text{total}}$  as in eq.(2.1). Further, such a setting corresponds to the situation that the supercurrent flowing in the left side varies in the situation that the supercurrent flowing in the right side are constant. We have described the validity for giving the values of each supercurrent flowing in the left and the right sides by hand in subsection.2.2. Since the values of the supercurrents are set, the phase differences are determined, which determine the magnetic flux penetrating the circuit of the SQUID, from Table.1. Then, from the information of the values of the supercurrents and the magnetic flux, we can read out the relation between the total current  $J_{\text{total}}$  given in eq.(2.1) and the magnetic flux induced by the supercurrents flowing in the circuit.

As a result, we can obtain the maximum amplitude of the supercurrent flowing into the circuit  $J_{\text{max}}$  given in eq.(2.3) against the magnetic flux  $\Phi$  as in Fig.8. As can be seen from eq.(2.3),  $|J_{\text{max}}|$  is to be given as a cosine curve, and the result on the absolute cosine curve like Fig.8 is one of the specific behaviors in a SQUID. Here, we can see that Fig.8 is disparity. The reason for that disparity is simply that our actual

numerical data obtained in each Josephson junction as in Table.1 is in from about  $-\pi/2$  to  $\pi/2$  and the amount of the supercurrent in one side is fixed to a finite value.

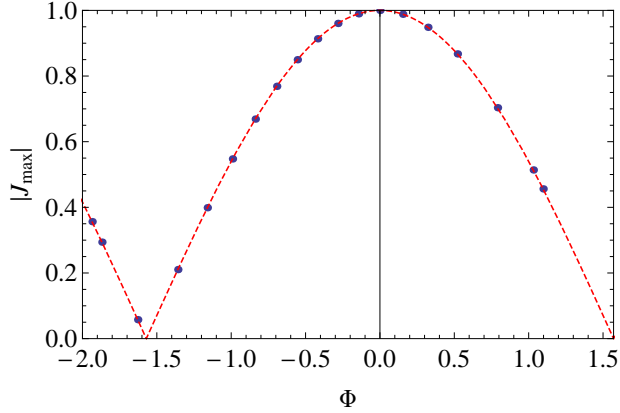


Figure 8: The blue points are our numerical result for the relation between the magnetic flux  $\Phi$  (x-axis) and the absolute value of the maximum amplitude of the supercurrent  $|J_{\max}|$  flowing into the circuit (y-axis). As can be seen from eq.(2.3),  $|J_{\max}|$  is to be given as a cosine curve, and the dashed line is the guide for the eye to show that our results are on an absolute cosine curve. The result on an absolute cosine curve like this figure is one of the specific behaviors in a SQUID. In the calculation to obtain this figure, we have varied the values of  $J_L$  as in Table.1 with a fixed  $J_R = -0.482052$  (This  $J_R$  means the current flowing from the top to the bottom in Fig.1, since we define the  $J_{\text{total}}$  as in eq.(2.1)), which means that the supercurrent flowing in the left side varies in the situation that the supercurrent flowing in the right side is constant. Here, we can see the disparity in this figure. The reason for that disparity is simply that our actual numerical data obtained in each Josephson junction as in Table.1 is in from about  $-\pi/2$  to  $\pi/2$ , and the amount of the supercurrent in one side is fixed to a finite value.

Finally, indeed we have also performed the another calculation, which takes the value of  $\nu(\chi)$  appearing in the expansion (3.10d) as the input of the calculation. Here, giving  $\nu(\chi)$  at first means considering the situation that the external magnetic flux exists from the beginning through eq.(2.4). In the actual calculation, The  $\nu(\chi)$  we have actually taken has been some constants. Then, we could not find any solutions. From this result, we can expect no configuration in constant external magnetic fluxes in the Josephson junction.

## Acknowledgment

I would like to thank the authors of that paper [25], Yong-Qiang Wang, Rong-Gen Cai and Hai-Qing Zhang. Particularly, I would like to thank Hai-Qing Zhang very much for a lot of discussions through email right to the end. I would also like to thank Li-Fang Li for her work in the very early stage of this study.

## Appendix A Numerical results used in Figs.7 and 8

We show explicitly the phase difference  $\gamma_{L,R}$  defined in eq.(4.1) obtained from solving the equations of motion (3.7a)-(3.7e) in each left and right space one by one by varying the value of the supercurrent  $J_{L,R}$  as the inputs and taking the chemical potential as in the right figure of Fig.4. Figs.7 and 8 are plotted based on these numerical results. Here, let us notice that we measure the phases in anticlockwise direction in Fig.1 and the relation between  $J_{\text{total}}$  and  $J_{L,R}$  are given eq.(2.1).

$\gamma_{L,R}$	$J_{L,R}/T_{\text{cH}}^2$		$\gamma_{L,R}$	$J_{L,R}/T_{\text{cH}}^2$
-1.51614	-1.21316		0.136253	0.160684
-1.45013	-1.20513		0.274963	0.321368
-1.20955	-1.12479		0.419009	0.482052
-0.939785	-0.964103		0.572359	0.642735
-0.741505	-0.803419		0.741505	0.803419
-0.572359	-0.642735		0.939785	0.964103
-0.419009	-0.482052		1.20955	1.12479
-0.274963	-0.321368		1.45013	1.20513
-0.136253	-0.160684		1.51614	1.21316
0	0			

Table 1: The Chebyshev Grid is taken for the all as  $(n_z, n_\chi) = (20, 35)$  but as  $(n_z, n_\chi) = (23, 43)$  for the ones  $J_{L,R}/T_{\text{cH}}^2 = \pm 1.21326$ . Here,  $n_z$  and  $n_\chi$  mean number of the grid in  $z$ - and  $\chi$ -directions, respectively. The critical temperature for the superconductor/normal metal transition  $T_{\text{cH}}$  is defined as  $T_{\text{cH}} = c\mu_{\text{H}}$  with  $c \equiv 0.0588$  [11].

## References

- [1] J. M. Maldacena, Adv. Theor. Math. Phys. **2**, 231 (1998) [hep-th/9711200].
- [2] S. S. Gubser, I. R. Klebanov and A. M. Polyakov, Phys. Lett. B **428**, 105 (1998) [arXiv:hep-th/9802109].  
E. Witten, Adv. Theor. Math. Phys. **2**, 253 (1998) [arXiv:hep-th/9802150].
- [3] S. S. Gubser, Phys. Rev. D **78**, 065034 (2008) [arXiv:0801.2977 [hep-th]].
- [4] S. A. Hartnoll, C. P. Herzog and G. T. Horowitz, Phys. Rev. Lett. **101**, 031601 (2008) [arXiv:0803.3295 [hep-th]].
- [5] S. A. Hartnoll, C. P. Herzog and G. T. Horowitz, JHEP **0812**, 015 (2008) [arXiv:0810.1563 [hep-th]].

- [6] S. -S. Lee, Phys. Rev. D **79**, 086006 (2009) [arXiv:0809.3402 [hep-th]].
- [7] H. Liu, J. McGreevy and D. Vegh, Phys. Rev. D **83**, 065029 (2011) [arXiv:0903.2477 [hep-th]].
- [8] M. Cubrovic, J. Zaanen and K. Schalm, Science **325**, 439 (2009) [arXiv:0904.1993 [hep-th]].
- [9] T. Nishioka, S. Ryu and T. Takayanagi, JHEP **1003**, 131 (2010) [arXiv:0911.0962 [hep-th]].
- [10] B. D. Josephson, Phys. Lett. **1**, 251 (1962).
- [11] G. T. Horowitz, J. E. Santos and B. Way, Phys. Rev. Lett. **106**, 221601 (2011) [arXiv:1101.3326 [hep-th]].
- [12] Y. -Q. Wang, Y. -X. Liu, R. -G. Cai, S. Takeuchi and H. -Q. Zhang, JHEP **1209**, 058 (2012) [arXiv:1205.4406 [hep-th]].
- [13] Y. -Q. Wang, Y. -X. Liu and Z. -H. Zhao, arXiv:1104.4303 [hep-th].
- [14] M. Siani, arXiv:1104.4463 [hep-th].
- [15] Y. -Q. Wang, Y. -X. Liu and Z. -H. Zhao, arXiv:1109.4426 [hep-th].
- [16] E. Kiritsis and V. Niarchos, JHEP **1107**, 112 (2011) [Erratum-ibid. **1110**, 095 (2011)] [arXiv:1105.6100 [hep-th]].
- [17] E. Nakano and W. -Y. Wen, Phys. Rev. D **78**, 046004 (2008) [arXiv:0804.3180 [hep-th]].
- [18] T. Albash and C. V. Johnson, JHEP **0809**, 121 (2008) [arXiv:0804.3466 [hep-th]].
- [19] S. A. Hartnoll and P. Kovtun, Phys. Rev. D **76**, 066001 (2007) [arXiv:0704.1160 [hep-th]].
- [20] O. Domenech, M. Montull, A. Pomarol, A. Salvio and P. J. Silva, JHEP **1008**, 033 (2010) [arXiv:1005.1776 [hep-th]].
- [21] M. Montull, O. Pujolas, A. Salvio and P. J. Silva, Phys. Rev. Lett. **107**, 181601 (2011) [arXiv:1105.5392 [hep-th]].
- [22] A. Salvio, J. Phys. Conf. Ser. **442**, 012040 (2013) [arXiv:1301.0201].
- [23] M. Montull, O. Pujolas, A. Salvio and P. J. Silva, JHEP **1204**, 135 (2012) [arXiv:1202.0006 [hep-th]].
- [24] R. -G. Cai, L. Li, L. -F. Li, H. -Q. Zhang and Y. -L. Zhang, Phys. Rev. D **87**, 026002 (2013) [arXiv:1209.5049 [hep-th]].

- [25] R. -G. Cai, Y. -Q. Wang and H. -Q. Zhang, arXiv:1308.5088 [hep-th].
- [26] G. T. Horowitz and R. C. Myers, Phys. Rev. D **59**, 026005 (1998) [hep-th/9808079].
- [27] S. Nakamura, Prog. Theor. Phys. **119**, 839 (2008) [arXiv:0711.1601 [hep-th]].
- [28] Lloyd N. Trefethen, *Spectral Methods in MATLAB*, SIAM, Philadelphia, 2000.